Linear Time Computation of QFT Feasible Regions

M. Sami Fadali
Electrical Engineering
University of Nevada
Reno, NV 89557
email: fadali@ee.unr.edu

L. LaForge
Embry-Riddle Aeronautical Univ.
Naval Air Station
Fallon, NV 89407
Larry@The-Right-Stuff.com

F. Harris, Jr.
Computer Science
University of Nevada
Reno, NV 89557
fredh@cs.unr.edu

Abstract

This paper represents ongoing research to reduce the computational cost of implementations of quantitative feedback theory (QFT), using ideas from Kharitonov stability theory and the theory of algorithms. By limiting our analysis to the simple case of a plant transfer function with denominator uncertainty, we gain insight into the problem of determining tracking, robust stability and actuator bounds for QFT design. A coordinate transformation allows us to exploit symmetry to reduce the computational time for the problem. This approach can be applied to more general uncertainty structures and is a main contribution of this paper. Our analysis demonstrates the importance of estimating asymptotic bounds on computational time, as is standard in algorithmic analysis. We obtain a linear time algorithm by dividing the compensator plane into twelve different regions, each of which shares critical points of a value set needed in the computation of QFT bounds. We illustrate our algorithm with a simple position control system.

I. Introduction

Quantitative feedback theory (QFT) is an integrated design methodology that allows the design of tracking controllers in the presence of parameter uncertainty. As originally proposed, QFT required extensive experience to obtain good results [1]. Today, computer programs have made this methodology accessible to the practicing control engineer [2]. However, the computational cost of QFT becomes prohibitive as the number of uncertain parameters increases. Several researchers have developed algorithms to reduce the time required to calculate the bounds used in QFT design [3], [4], [5]. In [3], the use of value sets known from Kharitonov stability theory [6] allowed the authors to compute the tracking bounds for affine uncertainty in the numerator and denominator. In [4], a major simplification in QFT design is achieved by relying on sensitivity or complementary sensitivity bounds rather than tracking bounds.

Fadali and LaForge [5] introduce the notation and methods of algorithmic analysis in the context of QFT bounds. For the sake of illustration, the analysis was restricted to the simple case of a system with denominator uncertainty and a numerator known with arbitrary accuracy. The paper emphasized that, to assess the usefulness of control algorithms, it is important 1) to formally prove their correctness, as is standard practice in the design of algorithms, and 2) to obtain asymptotic bounds on running time.

A key observation, used in both [3] and [5], is that the magnitude of the sum of a test compensation value (complex number) and a plant value set can be considered as the distance between the value set and the negative of the compensation value. The tracking bound for QFT can therefore be viewed as an upper bound on the ratio of the maximum distance to the minimum distance to the value set. Similarly, the stability robustness bound can be viewed as a lower bound on the distance to the value set. In this paper we further examine the problem addressed in [5], refining the same observation concerning distances. We show that, in special cases, the complex plane can be divided into regions where the farthest and closest points of the value set remain unchanged. A coordinate transformation simplifies the evaluation of both the stability robustness and tracking bounds by reducing the problem to one where the bounds are symmetric about the value set. The inverse transformation yields the required bounds, and the entire computation is achieved in constant time.

While the subdivision of the complex plane and the coordinate transformation are applied here to the simple problem solved in [5], the same approach can be applied to more complicated uncertainties. Application to systems with numerator interval polynomials and to affine numerator and denominator are topics for further research. Our results are also useful if the modified QFT design approach of [4] is adopted.

The paper is organized as follows. First we examine tracking and stability robustness bounds for a system with denominator uncertainty. We show that the complex plane can be divided into twelve regions each of which has a fixed farthest and closest point in the rectangular value set. We then introduce the coordinate transformation that simplifies the computation of the required QFT bounds. Next, we compare the computational time [7] of the new algorithm as compared to [5] and to the standard gridding approach [8]. Finally, we illustrate the action of our algorithm with a simple position control system.

II. QFT Bounds

Consider a single-input-single-output system comprised of a plant and a feedback compensator. The closed-loop transfer function (CLTF) for the system is given by

$$\left|T(\omega)\right| = \frac{1}{\left|P^{-1}(j\omega, p, q) + K(j\omega)\right|} \tag{1}$$

where P is the uncertain plant transfer function, K is a compensator transfer function, and p and q are vectors of uncertain parameters for the numerator and denominator polynomials, respectively. Because we are primarily interested in exploring the development of new computational tools for QFT bounds, we focus our attention on the simplest meaningful problem for which those tools can be explored. We consider the case of a plant transfer function with denominator uncertainty, *i.e.*

$$P(j\omega, p, q) = \frac{N(j\omega)}{D(j\omega, q)} \tag{2}$$

The maximum CLTF magnitude is therefore given by

$$\left|T(\omega)\right|_{\max} = \frac{\left|N(j\omega)\right|}{\min\limits_{q}\left|D(j\omega, q) + KN(j\omega)\right|} \tag{3}$$

while the minimum CLTF magnitude is

$$\left|T(\omega)\right|_{\min} = \frac{\left|N(j\omega)\right|}{\max\limits_{q}\left|D(j\omega, q) + KN(j\omega, p)\right|} \tag{4}$$

The worst-case magnitude ratio is

$$\frac{\left|T(\omega)\right|_{\max}}{\left|T(\omega)\right|_{\min}} = \frac{\max\limits_{q}\left|D(j\omega, q) + KN(j\omega)\right|}{\min\limits_{q}\left|D(j\omega, q) + KN(j\omega)\right|} \tag{5}$$

Let $C = x_c + j\, y_c$ be the product of K and N and rewrite (5) as

$$\frac{\left|T(\omega)\right|_{\max}}{\left|T(\omega)\right|_{\min}} = \frac{\max\limits_{q}\left|D(j\omega, q) + C(j\omega)\right|}{\min\limits_{q}\left|D(j\omega, q) + C(j\omega)\right|} \tag{6}$$

It will be convenient to re-express C in Cartesian coordinates as (x_C, y_C), and write (6) in the form

$$\frac{\left|T(\omega)\right|_{\max}}{\left|T(\omega)\right|_{\min}} = \frac{\max\limits_{q}\left|D(j\omega, q) - C_m(j\omega)\right|}{\min\limits_{q}\left|D(j\omega, q) - C_m(j\omega)\right|} \tag{7}$$

where $C_m = -C = (-x_c, -y_c) = (x, y)$. We now observe that the magnitudes in equations (3) through (7) involve distances between the values of the complex number D and the complex number C_m [3]. Thus the problem of determining QFT tracking bounds is equivalent to determining the ratio of the maximum to minimum distance between the point C_m and the set D.

In addition, robust stability requires that

$$\left|T(\omega)\right|_{\max} = \frac{\left|N(j\omega)\right|}{\min\limits_{q}\left|D(j\omega,q)-C_m\right|} \le M_p \tag{8}$$

i.e.

$$\min_{q}\left|D(j\omega,q)-C_m\right| \ge \frac{\left|N(j\omega)\right|}{M_p} \tag{9}$$

In the case of cascade compensation, (7) is unchanged, but the right hand side of (9) is multiplied by $|K|$. Similarly, the lower bound

$$\left|T(\omega)\right|_{mi} = \frac{\left|N(j\omega)\right|}{\min\limits_{q}\left|D(j\omega,q)-C_m\right|} \ge M_l \tag{10}$$

is equivalent to the condition

$$\min_{q}\left|D(j\omega,q)-C_m\right| \le \frac{\left|N(j\omega)\right|}{M_l} \tag{11}$$

Let D be the nth order interval polynomial

$$D(s;\, q) = a_n(q)\, s^n + a_{n-1}(q)\, s^{n-1} + \ldots + a_0(q) \tag{12}$$

with uncertainty bounds $a_i \in \left[a_i^-, a_i^+\right]$, $i = 0, 1, \ldots, n$. Then the value set associated with the uncertain polynomial is the Kharitonov rectangle $D^{\square}$ with generating polynomials [6]

$$\begin{aligned}
D^{++}(s) &= a_0^+ + a_1^+ s + a_2^-\, s^2 + a_3^-\, s^3 + \cdots \\
D^{+-}(s) &= a_0^+ + a_1^- s + a_2^-\, s^2 + a_3^+\, s^3 + \cdots \\
D^{-+}(s) &= a_0^- + a_1^+ s + a_2^+\, s^2 + a_3^-\, s^3 + \cdots \\
D^{--}(s) &= a_0^- + a_1^- s + a_2^+\, s^2 + a_3^+\, s^3 + \cdots
\end{aligned} \tag{13}$$

Refer to Figure 1; $(x, y) \in D^{\square}$ if and only if

$$x_- \le x \le x_+ \tag{14a}$$
$$y_- \le y \le y_+ \tag{14b}$$

where x_+ (*resp.* x_-) denotes the real component of D^{++} (*resp.* D^{--}) and y_+ (*resp.* y_-) denotes the imaginary component of D^{++} (*resp.* D^{--}).

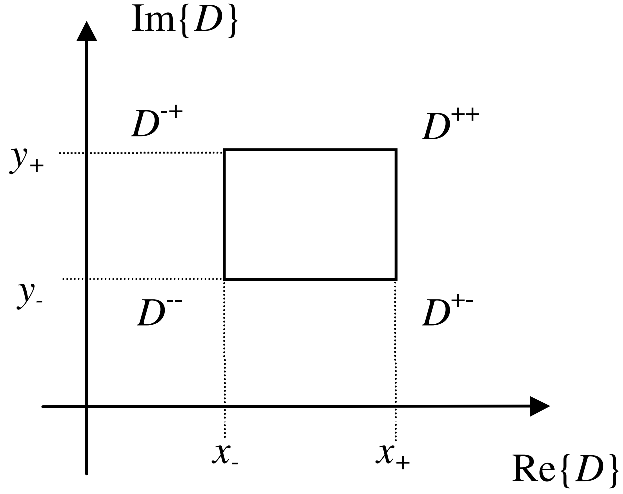

Fig. 1 Kharitonov rectangle $D^{\square}$.

Algorithmic computation of the worst-case ratio is now tractable because, as we show, the maximum and minimum magnitude corresponds to an extreme point of the value set $D^{\square}$, or to a point on an edge of $D^{\square}$.

III. Determination of Maximum and Minimum Distance

To determine the stability robustness and tracking bounds for a system of denominator uncertainty, we obtain the maximum and minimum distances between a test point $C_m = (x, y)$ in the complex plane and the Kharitonov rectangle $D^{\square}$. Figure 2 shows a test point and the Kharitonov rectangle in the complex plane. We use the notation

$$\left(x_{av}, y_{av}\right) = \left(\frac{x_- + x_+}{2}, \frac{y_- + y_+}{2}\right) \tag{15}$$

The plane can be divided into regions 1, 2, …, 12. Within region *i,* there is a unique point $(\hat{x}, \hat{y}) \in D^{\square}$ at maximum distance from C_m and a unique point $(\breve{x}, \breve{y}) \in D^{\square}$ at minimum distance. We exclude from consideration the interior of the Kharitonov rectangle, since the interior corresponds to unstable systems. The twelve regions have properties summarized by Table 1 and established by the following theorem.

Theorem 1. Let $D^{\square}$ be a rectangular region and (x, y) a test point. The furthest point $(\hat{x}, \hat{y}) \in D^{\square}$ to (x, y) and the closest point $(\breve{x}, \breve{y}) \in D^{\square}$ to (x, y) are as given in Table 1.

Proof

The distance $D^{\square}$ to (x, y) is maximized or minimized by separately maximizing

$$\left(x - \hat{x}\right)^2 \qquad and \qquad \left(y - \hat{y}\right)^2$$

or minimizing

$$\left(x - \breve{x}\right)^2 \qquad and \qquad \left(y - \breve{y}\right)^2$$

respectively; *i.e.*, minimizing the distance in the horizontal and vertical directions separately.

For the horizontal direction, $(x-\hat{x})^2$ is maximized in Regions 1, 2, 5, 6, 7 and 12, at $\hat{x}=x_+$, and in Regions 3, 4, 8, 9, 10 and 11, at $\hat{x}=x_-$. $(x-\breve{x})^2$ is minimized in Regions 1, 2, 5 and 6, at $\breve{x}=x_-$, and in Regions 3, 4, 9 and 10, at $\breve{x}=x_+$. In Regions 7, 8, 11 and 12, a minimum value of zero is possible with $\breve{x}=x$.

■

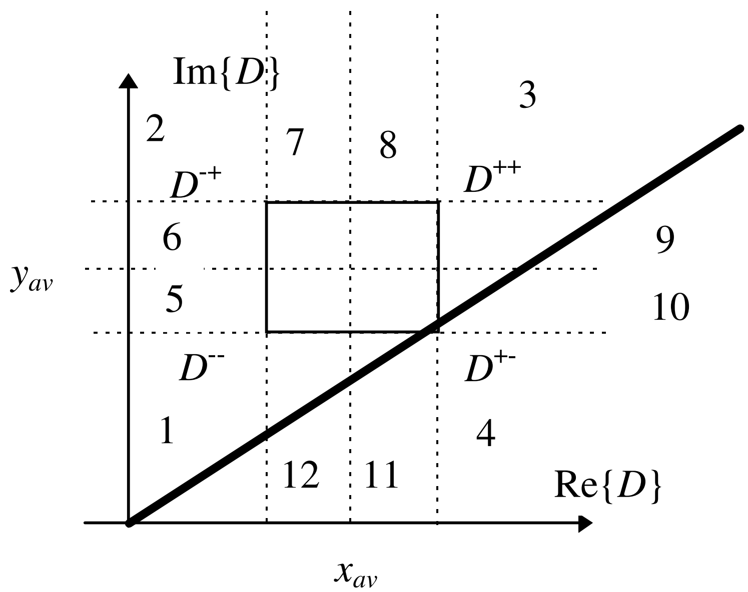

Fig. 2 Twelve regions for the determination of the maximum and minimum distances to the point (x, y).

Table 1 Properties of regions traversed by radial lines.

Region No.	Boundary	$(\hat{x},\hat{y})$	$(\breve{x},\breve{y})$
1	$x < x_-$ & $y < y_-$	(x_+, y_+)	(x_-, y_-)
2	$x < x_-$ & $y > y_+$	(x_+, y_-)	(x_-, y_+)
3	$x > x_+$ & $y > y_+$	(x_-, y_-)	(x_+, y_+)
4	$x > x_+$ & $y < y_-$	(x_-, y_+)	(x_+, y_-)
5	$x < x_-$ & $y \in [y_-, y_{av}]$	(x_+, y_+)	(x_-, y)
6	$x < x_-$ & $y \in [y_{av}, y_+]$	(x_+, y_-)	(x_-, y)
7	$x \in [x_-, x_{av}]$ & $y > y_+$	(x_+, y_-)	(x, y_+)
8	$x \in [x_{av}, x_+]$ & $y > y_+$	(x_-, y_-)	(x, y_+)
9	$x > x_+$ & $y \in [y_{av}, y_+]$	(x_-, y_-)	(x_+, y)
10	$x > x_+$ & $y \in [y_-, y_{av}]$	(x_-, y_+)	(x_+, y)
11	$x \in [x_{av}, x_+]$ & $y < y_-$	(x_-, y_+)	(x, y_-)
12	$x \in [x_-, x_{av}]$ & $y < y_-$	(x_+, y_+)	(x, y_-)

For each region the tracking bound is defined by

$$R^2 = \frac{(x-\hat{x})^2 + (y-\hat{y})^2}{(x-\breve{x})^2 + (y-\breve{y})^2} \le B^2 \tag{16}$$

with $B > 1$. At the boundary in Regions 1 through 4 we have

$$\begin{aligned} &\left(B^2-1\right)x^2 - 2x\left(B^2\breve{x}-\hat{x}\right) + \left(B^2\breve{x}^2-\hat{x}^2\right) \\ &+\left(B^2-1\right)y^2 - 2y\left(B^2\breve{y}-\hat{y}\right) + \left(B^2\breve{y}^2-\hat{y}^2\right) = 0 \end{aligned} \tag{17}$$

with the feasible region outside the boundary. Completing the square gives the equation of a circle with center (c_x, c_y) and radius c_r

$$\left(x-c_x\right)^2 + \left(y-c_y\right)^2 = c_r^2 \tag{18}$$

where

$$\begin{aligned} c_x &= \frac{B^2\breve{x}-\hat{x}}{B^2-1} \\ c_y &= \frac{B^2\breve{y}-\hat{y}}{B^2-1} \\ c_r &= \frac{B}{B^2-1}\sqrt{(\hat{x}-\breve{x})^2 + (\hat{y}-\breve{y})^2} \end{aligned} \tag{19}$$

In Regions 5 through 12, one of the quadratic terms in (17) vanishes. In Regions 7, 8, 11 and 12, condition (17) reduces to

$$\left(B^2-1\right)y^2 - 2y\left(B^2\breve{y}-\hat{y}\right) - (x-\hat{x})^2 + \left(B^2\breve{y}^2-\hat{y}^2\right) = 0 \tag{20}$$

Completing squares, we have the equation of the hyperbola

$$-\frac{(x-\hat{x})^2}{\mathrm{c}_{ry}^2\left(B^2-1\right)} + \frac{\left(y-c_y\right)^2}{\mathrm{c}_{ry}^2} = 1 \tag{21}$$

where $\mathrm{c}_{ry} = B\left|\hat{y}-\breve{y}\right| / \left(B^2-1\right)$; that is, c_r with the x-related terms removed. The hyperbola is symmetric about axes through $\left(\hat{x}, c_y\right)$ has x-intercept at $\hat{x} \pm \sqrt{\mathrm{c}_{ry}^2\left(B^2-1\right)}$, and features asymptotes through $\left(\hat{x}, c_y\right)$ and $c_y \pm \mathrm{c}_{ry}$. In Regions 5, 6, 9 and 10, we have similar hyperbolas with x and y interchanged and $\mathrm{c}_{rx} = B\left|\hat{x}-\breve{x}\right| / \left(B^2-1\right)$; that is, c_r with the y-related terms removed.

Each boundary is only valid for the region for which the points $\left(\hat{x}, \hat{y}\right)$ and $\left(\breve{x}, \breve{y}\right)$ apply. In Regions 1 through 4, the outside of the circle is the allowable compensation where the ratio is less than the specified value. In the remaining regions, the allowable compensation is outside the hyperbolas.

The stability robustness bound is defined by

$$(x-\breve{x})^2 + (y-\breve{y})^2 \ge (N/M)^2 \tag{22}$$

So the boundary is a circle of center $(\breve{x}, \breve{y})$ and radius *N*/*M* and the allowable region is outside the circle.

The actuator bound is due to the maximum allowable compensation magnitude $\gamma_{\max}$ at each frequency. It is defined by

$$x^2 + y^2 \leq \gamma_{\max}^2 \tag{23}$$

This boundary is a circle centered at the origin with radius $\gamma_{\max}$ and the allowable region is inside the circle.

Theorem 2. Let $(\hat{x}, \hat{y})$ and $(\breve{x}, \breve{y})$ be known for a system with an interval polynomial in the denominator and a fixed numerator. The QFT boundaries and the feasible compensation regions are given by

1) In Regions 1 through 4 the tracking boundary is a circle of radius c_r, centered at $(-c_x, -c_y)$, with the feasible region outside the boundary. In Regions 7, 8, 11 and 12, the tracking boundary is a hyperbola, symmetric with respect to axes through $(-\hat{x}, -c_y)$, and having horizontal intercept at $-\hat{x} \pm \sqrt{B^2-1}$ and asymptotes through $(-\hat{x}, -c_y)$ and $-c_y \pm c_r$. In Regions 5, 6, 9, and 10, the tracking boundary is a hyperbola, symmetric with respect to axes through $(-c_x, -\hat{y})$, and having horizontal intercept at $-\hat{y} \pm \sqrt{B^2-1}$ and asymptotes through $(-c_x, -\hat{y})$ and $-c_x \pm c_{rx}$.

2) The stability robustness boundary is a circle of radius *N*/*M* centered at $(-\breve{x}, -\breve{y})$ with the feasible region outside the boundary.

3) The actuator boundary is a circle of radius $\gamma_{\max}$ centered at the origin with the feasible region inside the boundary.

Proof
The results are obtained on replacing (x, y) by $(-x, -y)$ in (16), (17), and (18).

■

Remark 1. Theorem 2 is only valid if the farthest and closest points in the Kharitonov rectangle to a test point are fixed. In each of Regions 5 through 12 this is not the case. The result is that the robust stability boundaries for these regions comprise *straight lines* parallel to the adjacent edge of Kharitonov rectangle and tangent to the set of circles corresponding to the region. This conclusion and others are much more easily reached by transforming the problem as described in the next section.

III. Coordinate Transformation to Simplify Bound Computation

In this section we describe a coordinate transformation to reduce the subdivision of the complex plane for QFT boundary calculation to one where we have symmetry. This symmetry can be exploited to reduce computation. We transform the compensation to (x, y) using

$$\begin{bmatrix} x \\ y \end{bmatrix} = -\begin{bmatrix} x_c \\ y_c \end{bmatrix} - \begin{bmatrix} x_{av} \\ y_{av} \end{bmatrix} \leftrightarrow \begin{bmatrix} x_c \\ y_c \end{bmatrix} = -\begin{bmatrix} x \\ y \end{bmatrix} - \begin{bmatrix} x_{av} \\ y_{av} \end{bmatrix} \tag{24}$$

The transformed region has as its origin the center of the Kharitonov rectangle as shown in Figure 3. Only the three regions where x and y are both positive need be considered, because of the symmetry resulting from the transformation. For each point (x, y) on a boundary, symmetry yields the set of boundary points

$$\{(x, y), (-x, y), (x, -y), (-x, -y)\}$$

Transforming back to the original coordinates, we have the four points

$$\{(-x-x_{av}, -y-y_{av}), (x-x_{av}, -y-y_{av}), (-x-x_{av}, y-y_{av}), (x-x_{av}, y-y_{av})\}$$

We now give the equivalent of Theorem 1 for the transformed domain of (22).

Theorem 3. Let D' be a transformed rectangular region and (x, y) a test point. The farthest point $(\hat{x}, \hat{y})$ in D' to (x, y) and the closest point $(\breve{x}, \breve{y})$ in D' to (x, y) are given by Table 2.

Proof
The proof is similar to that for of Theorem 1, where $x_f = (x_+ - x_-)/2$ and $y_f = (y_+ - y_-)/2$.

Table 2. Closest and farthest points for the transformed domain.

Region	$(\breve{x}, \breve{y})$	$(\hat{x}, \hat{y})$
I	(x, y_f)	$(-x_f, -y_f)$
II	(x_f, y_f)	$(-x_f, -y_f)$
III	(x_f, y)	$(-x_f, -y_f)$

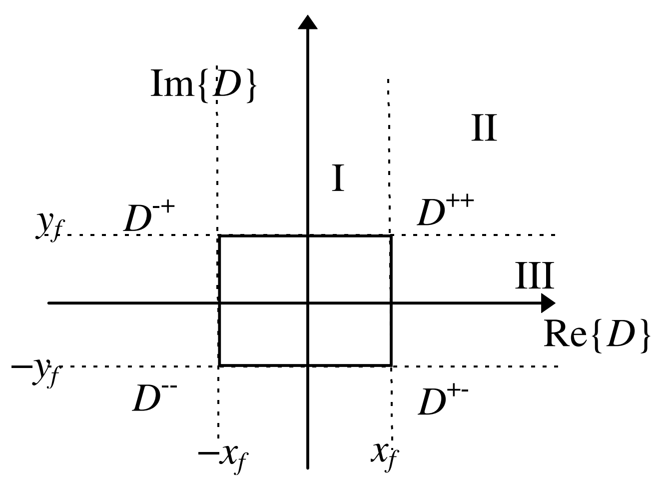

Fig. 3 The transformed Kharitonov rectangle.

We assume that we remain in a single region so that the points for maximum and minimum distances are fixed. This allows us to derive the following properties.

Theorem 4. As x or y vary in Region I or III, the real-valued function (1) is monotone increasing. As x or y vary in Region I or III, the value of (1) is unimodal.

Proof
Differentiate the middle expression in (16) and equate to zero. For Region I, $\breve{x} = x$ and $\widehat{x} = -x_f$, so that (16) reduces to

$$R^2 = \frac{\left(x + x_f\right)^2 + \left(y + y_f\right)^2}{\left(y - y_f\right)^2} \le B^2$$

Differentiating with respect to *x* and equating to zero, we obtain

$$\tfrac{1}{2}\frac{\partial R^2}{\partial x} = \frac{x + x_f}{\left(y - y_f\right)^2} = 0$$

This indicates a positive derivative with the inadmissible negative root $x = -x_f$.

Differentiating with respect to *y* and equating to zero, we obtain

$$\tfrac{1}{2}\frac{\partial R^2}{\partial y} = \frac{\left(y + y_f\right)\left(y - y_f\right) - \left[\left(y + y_f\right)^2 + \left(x + x_f\right)^2\right]}{\left(y - y_f\right)^3} = 0$$

$$\left(x + x_f\right)^2 + 2y_f\left(y + y_f\right) = 0$$

This indicates a positive derivative with the inadmissible negative root

$$y = -y_f - \frac{\left(x + x_f\right)^2}{2y_f}$$

Because the derivatives are positive and have no positive real roots we conclude that the function is montone increasing.

Interchanging *x* and *y* establishes monotonicity of (1) in Region III.

In Region II, $\breve{x} = x_f$ and $\widehat{x} = -x_f$, so that (16) becomes

$$R^2 = \frac{\left(x + x_f\right)^2 + \left(y + y_f\right)^2}{\left(x - x_f\right)^2 + \left(y - y_f\right)^2} \le B^2$$

$$\begin{aligned}\tfrac{1}{2}\frac{\partial R^2}{\partial x} &= \frac{\left(x + x_f\right)\left[\left(x - x_f\right)^2 + \left(y - y_f\right)^2\right] - \left(x - x_f\right)\left[\left(x + x_f\right)^2 + \left(y + y_f\right)^2\right]}{\left[\left(x - x_f\right)^2 + \left(y - y_f\right)^2\right]^2} \\ &= \frac{-2x_f\left(x^2 - x_f^2\right) - 4yy_f x + 2x_f\left[y^2 + y_f^2\right]}{\left[\left(x - x_f\right)^2 + \left(y - y_f\right)^2\right]^2} = 0\end{aligned}$$

This yields the roots

$$x = -\frac{yy_f}{x_f} \pm \sqrt{\left(\frac{yy_f}{x_f}\right)^2 + y^2 + y_f^2 + x_f^2} \tag{25}$$

One root is negative and is therefore inadmissible. The second root is greater than x_f and is therefore inside Region 2. Therefore, the function (1) is unimodal in Region 2. For large x the function (1) approaches its minimum value of unity. We conclude that, in Region II, the nonfeasible region is in the vicinity of a maximum of the ratio R^2 as shown in Figure 4. Because the value of R^2 as $x \to x_f$ may be larger than B^2, the intersection of the curve of Figure 4 with the line $R^2 = B^2$ may occur at either *one or two points*.

■

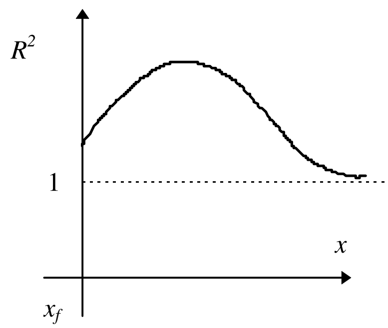

Fig.4 Unimodal function in Region II.

We now examine the boundaries of Theorem 2 for the transformed domain. The coordinate transformation is linear and the boundaries retain their form. In terms of the stability robustness boundary, however, the transformation reveals the following.

Theorem 5. The stability robustness boundary for the transformed domain in Regions I and II comprises straight lines parallel to the edges of the Kharitonov rectangle. In Region II, the boundary is a circle of radius N/M centered at (x_f, y_f).

Proof

The stability robustness bound is given by (20) with $(\breve{x}, \breve{y})$ defined for Regions I, II, and III. In Region I, $(\breve{x}, \breve{y}) = \left(x, y_f\right)$ and the boundary is the vertical straight line

$$y = y_f + N/M$$

Similarly, in Region III, the boundary is the vertical line

$$x = x_f + N/M$$

In Region II, $(\breve{x}, \breve{y}) = \left(x_f, y_f\right)$ and the boundary is the circle

$$\left(y - y_f\right)^2 + \left(x - x_f\right)^2 = \left(N/M\right)^2$$

i.e., a circle of radius N/M centered at (x_f, y_f).

■

Remark 2. Transforming the rectangle using the inverse transformation of (24) gives a second rectangle centered at $(-x_{av}, -y_{av})$. The symmetry revealed in the transformed domain holds in the vicinity of the rectangle in the original coordinates. Based on this observation, the boundaries and feasible region of compensation can be easily plotted, as demonstrated in the following sections.

V. An Optimal, Linear Time Algorithm for Computing the Feasible Region of Compensation

We are now in a position to state the main algorithmic result of this paper. In (2), let the order of the numerator polynomial N be m and the order of the uncertain denominator polynomial D be n. Horner's Rule evaluates these polynomials in time $\theta(m)$ *resp.* $\theta(n)$ (Cormen *et al.*, [7] 1993, ex. 1.2-4). The numerator need be evaluated only once, but, in order to compute the Kharitonov rectangle, the denominator is recomputed (in optimal time $\theta(n)$) for each of n_w sample frequencies ω. For fixed ω, Theorem 2 prescribes how to determine, in optimal time $\theta(1)$, a set of constraints defining the feasible region of compensation. Thus, in time $\theta(n_w n + m)$, the frequency-divided boundary of minimum magnitude compensations can be computed. When, as is often the case, $n_w n$ is much greater than m, the running time is $\theta(n_w\ n)$. This compares favorably with the $\theta(n_w n_\gamma n_\phi n)$ running time of [5] and is certainly preferable to the $\theta(n_q n_w n_\gamma n_\phi n)$ running time of the traditional gridding approach [8], where n_q is the total number of grid points in the uncertain parallelpiped Q, n_γ is the number of grid points along the axis of compensation magnitude, and n_ϕ is the number of points along the compensation phase axis. Since the numerator need be evaluated only once, the Rule of Products implies that the search as described runs in time $\theta(n_q n_w n_\gamma n_\phi n + m)$.

To demonstrate the reduction in computational time achieved here, we examine the case of a plant transfer function with six uncertain parameters and ten grid points for each parameter; *i.e.*, $n_q = 10^6$. For $n_\gamma = n_\phi = 10$, the overall reduction achieved here is by a factor of one hundred when compared to [5] and 10^8 when compared to the traditional gridding method.

VI. Examples

Example1: Position Control System

Consider the position control system with motor and load transfer function

$$G(s) = \frac{10}{s(\tau s + 1)}$$

where $\tau \in [\tau_{\min}, \tau_{\max}]$. For the compensator K, the product of the numerator of the transfer function and the compensator is $C = 10\,K$. The denominator is an interval polynomial whose value set at any frequency ω is the interval $[-\tau_{\max}\omega^2, -\tau_{\min}\omega^2]$ on the straight line parallel to the real axis, with imaginary intercept ω. In this simple case, the twelve regions of Figure 2 reduce to 6 and the three regions of Figure 4 reduce to two. The bounds for the system are shown in Figure 5, together with the value set for a frequency of 1 rad/s.

For this example, c_{ry} is zero and the hyperbolas for Regions 7, 8, 11 and 12 reduce to a single point outside the respective regions. Regions 5, 6, 9 and 10 are not defined for the example and need not be considered. In Regions 1 through 4 the tracking boundaries are circular arcs with the feasible region outside the arcs. The stability robustness boundary comprises circular arcs of radius N/M = 10/2 = 5 and straight lines parallel to the value set. The actuator bound is a circle of radius γ_{act}. The feasible region for compensation is inside the actuator boundary and outside both the tracking boundary and the stability robustness boundary.

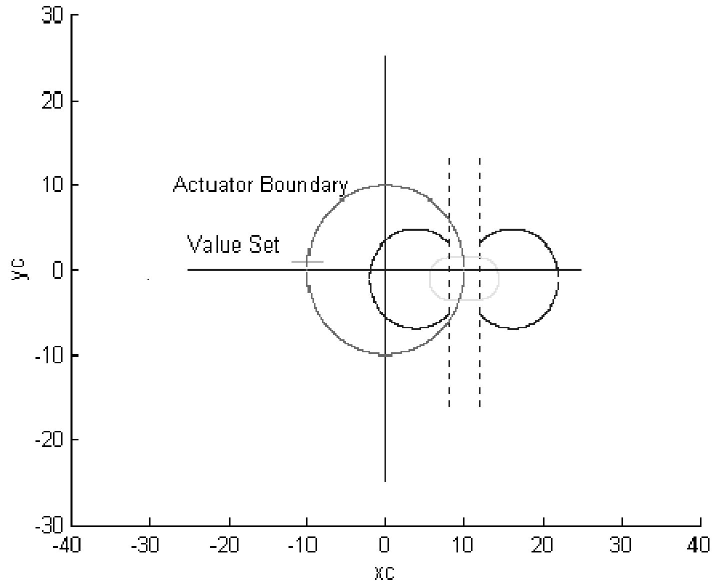

Fig. 5 QFT boundaries for the position control system.

Example 2: Two-parameter Uncertainty

Consider the transfer function

$$G(s) = \frac{1}{a_2 s^2 + a_1 s + 1}$$

where $a_i \in [\, a_i^-, a_i^+]$, i =1, 2. For $G(j\omega)$, the x and y coordinates of the denominator are in the ranges

$$x \in \; [1 - a_2^+\omega^2, 1 - a_2^-\omega^2], \;\; y \in \; [a_1^-\omega, \; a_1^+\omega]$$

The QFT bounds are shown in Figure 6. The permissible region is inside the circle obtained from the actuator bounds, inside the tracking bounds made up of hyperbolic and circular segments and outside the robust stability bounds. A design point can be selected for each point on the frequency grid. The set of design points can then be fitted with a compensator. Finally, the compensated system must be checked to determine if all design constraints are satisfied. It is also possible to add the bounds of the form (10) to Figure 6 so that the designer can attempt to satisfy all design constraints with a single compensator. If successful, 2-degree-of-freedom control with the added cost of a prefilter can be avoided. If not, the additional bound can be ignored and a loop compensator can be designed. Then a prefilter can be added to achieve the desired performance.

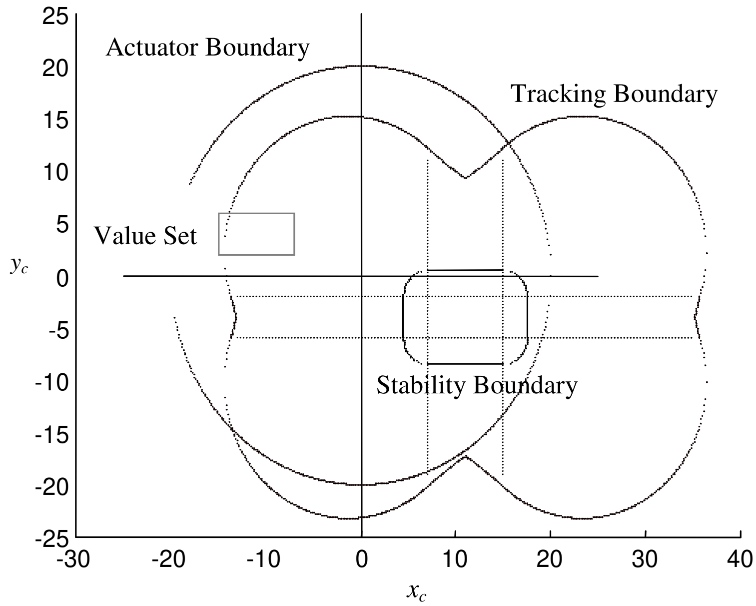

Fig. 6 QFT boundaries for the two-parameter system.

VII. Conclusion

This paper demonstrates the considerable computational saving possible in the computation of QFT bounds using value sets, coordinate transformations, and subdivisions of the compensator plane. Given a region where the farthest and closest points in the value set to a test point are determined, closed-form expressions for the boundaries can be calculated. This allows the computation of the QFT bounds in time $\theta(n_w\ n)$.

For a system with a numerator interval polynomial, a similar approach is possible with the distances sought being between two rectangular regions. For affine numerator and denominator polynomials, we seek the minimum and maximum distances between two polygons. These problems present challenges for future research.

References

[1] D'Azzo, J. J., and C. H. Houpis (1988). *Linear Control System Analysis and Design*. McGraw-Hill Book Company, New York.
[2] Borghesani, C., Y. Chait and O. Yaniv (1994). *Quantitative feedback theory toolbox*. The Mathworks Inc., Natick, MA.
[3] Brown, M. and I. R. Peterson (1991). Exact computation for the Horowitz bound for interval plants. *30th CDC*, Brighton, England, pp. 2268-2273.
[4] Rodriguez, G. M., Y. Chait and C. V. Hollot (1995). A new algorithm for computing QFT bounds. *Proc. 1995 ACC*, Seattle, WA
[5] Fadali, M. S., and LaForge, L., Algorithmic Analysis of Geometrically Computed QFT Bounds, *Proc. 1996 IFAC World Congress*, Vol. H, pp. 297-302. San Francisco, CA, June, 1996.
[6] Barmish, B. K.(1994). *New Tools for Robustness of Linear Systems*. Macmillan, NY, NY.
[7] Cormen, T. H., Leiserson, C. E. and R. L. Rivest (1993). *Introduction to Algorithms*. McGraw Hill, NY, NY.
[8] El-Zayyat, K.(1994). *VSC/QFT Robust Design of Systems with Bounded Uncertainties*, Ph. D. Dissertation, (M. S. Fadali, Advisor), UNR, Reno, NV.